Journal of Catalysis 263 (2009) 155–166

Contents lists available at ScienceDirect

Journal of Catalysis

www.elsevier.com/locate/jcat

Active sites on Cu/SiO_2 prepared using the atomic layer epitaxy technique for a low-temperature water–gas shift reaction

Ching-Shiun Chen [a,*], Jarrn-Horng Lin [b], Tzu-Wen Lai [a], Bao-Hui Li [b]

[a] Center for General Education, Chang Gung University, 259 Wen-Hwa 1st Road, Kwei-Shan Tao-Yuan, 333, Taiwan, ROC
[b] Department of Material Science, National University of Tainan, 33, Sec. 2, Shu-Lin St., Tainan, 700, Taiwan, ROC

ARTICLE INFO

Article history:
Received 13 November 2008
Revised 9 February 2009
Accepted 9 February 2009
Available online 27 February 2009

Keywords:
Atomic layer epitaxy
Copper
Water–gas shift reaction
Infrared spectroscopy
Temperature-programmed desorption
Carbon monoxide adsorption

ABSTRACT

The atomic layer epitaxy (ALE) technique has been used to prepare uniform copper nanoparticles dispersed on a silica support (ALE-Cu/SiO_2 with 2.85 ± 0.32 nm), which are highly active in the water–gas shift reaction. Infrared spectra of CO adsorption are employed to study the active sites on ALE-Cu/SiO_2 surface, suggesting that two major active sites are found on the copper surface, namely defect sites and highly dispersed Cu particles and/or isolated Cu atoms sites. We report here that the defect sites on these small Cu particles or isolated Cu atoms provide high activity for the water gas shift reaction. The high efficiency of the water gas shift reaction on the ALE-Cu/SiO_2 catalyst may be ascribed to its strong activity in promoting H_2O dissociation. Nanoscale Cu particles may be involved in strong interactions with the SiO_2 support, leading to a partially electropositive state as a result of interactions with oxygen atoms at the surface of the support, even if the copper is reduced.

1. Introduction

The water–gas shift (WGS) reaction ($CO + H_2O \rightarrow H_2 + CO_2$) is used extensively in the conversion of fossil fuels to hydrogen [1–7]. In particular, the WGS reaction achieves the conversion of CO to CO_2, which is important when hydrogen is used as a clean fuel for proton-exchange membrane fuel cells (PEMFC) in view of the strong poisoning effect of CO on Pt-based anodes. Pt-group metals, such as Au or Cu, are used as effective catalysts for the WGS reaction because of their high levels of activity and stability [1–7]. However, Pt- and Au-based catalysts can often display more activity for WGS reactions than Cu-based catalysts [6,7]. On the other hand, the noble metals are recognized as a scarce resource as well as a limiting factor in the development of viable energy alternatives to petroleum. Because of the high cost of precious metals, some transition metals with high levels of catalytic activity for the WGS reaction have been evaluated as alternatives. For example, copper is a potential substitute for noble metals because of its low price and widespread use. Thus, if the limitation of the low activity of copper-based catalysts can be overcome, these could prove invaluable.

Recently, a new class of Cu catalysts, the so-called low-temperature WGS catalysts based on ceria, has been extensively investigated [8,9]. However, the related literature has not mentioned that the metal-ceria catalysts can provide activity for performing WGS reactions at room temperature. To date, small metallic particles have been viewed as a very active area in solid-state physics and chemistry. It has been noted that nanoparticles usually offer a larger surface-to-volume ratio and a higher concentration of partially coordinated surface sites compared to bulk materials, and consequently appear to possess different physical and chemical properties [10,11]. Several studies have mentioned that a size reduction of metals can cause some changes in the electronic structure and/or the distribution of surface sites, leading to enhanced catalytic activity [12–14].

Copper-based catalysts are frequently used in a variety of industrial hydrogenation processes, including methanol synthesis and the low-temperature water gas shift reaction. Nanoscale copper particles can be expected to exhibit catalytic behavior different from that of traditional Cu-based catalysts. Although copper nanoparticles have received considerable attention in many fields [10,11,15,16], few researchers have discussed the catalytic activity and characterization of nanoscale copper particles less than 4 nm in diameter.

The atomic layer epitaxy (ALE) technique is a surface-controlled, layer-by-layer process that deposits thin films at an atomic scale through self-limiting surface reactions [17]. This technique is currently in use for the preparation of some nanoscale metal catalysts, such as those based on Cr, Co, Ni, Pd, and Ru. These catalysts have been applied to several hydrogenation and dehydrogenation reactions [18–22]. We recently used ALE to prepare Cu nanoparticles on a SiO_2 support with an average diameter of 2.4–3.4 nm with a nar-

* Corresponding author. Fax: +886 32118700.
E-mail address: cschen@mail.cgu.edu.tw (C.-S. Chen).

0021-9517/$ – see front matter
doi:10.1016/j.jcat.2009.02.004

row size distribution (<10% root mean square diameter) [23,24]. In our previous study, we found that ALE-Cu/SiO_2 displayed very different characteristics from those of typical Cu-based catalysts [23]. The activity of Cu-based catalysts for the reverse water gas shift reaction has been found to be size-dependent. The ALE-Cu/SiO_2 catalyst can strongly bind CO and has sufficient thermal stability to resist the sintering of Cu particles under high-temperature conditions. This property imparts high catalytic activity for the conversion of CO_2 to CO in the reverse WGS reaction. On the other hand, the nanoscale Cu/SiO_2 catalysts can also display surprisingly high activity for the water gas shift and water dissociation reactions, in comparison with the 5.6 wt% Pt/SiO_2 and 10.3 wt% Cu/SiO_2 prepared by the impregnation method [24]. Nevertheless, the issue of size-dependence on nanoscale Cu particles has attracted little attention thus far. If properly developed, nanoscale copper catalysts could be much more economical and may even be able to replace noble metals for application in WGS reactions.

In the research reported herein, a Cu/SiO_2 catalyst with nanoscale copper particles was prepared using the ALE technique, and the newly developed copper catalysts were found to display dramatic activity for the WGS reaction at room temperature. Moreover, the active sites and chemical state of the ALE-Cu/SiO_2 catalyst are discussed in relation to the characterization and activity results of the WGS reaction.

2. Experimental

2.1. Catalyst preparation

The ALE-Cu/SiO_2 catalysts were prepared in F-120C ALE equipment (Microchemistry Ltd.). Growth experiments were performed in a flow-type reactor at low pressure, with nitrogen as the carrier gas. In each run, 2–3 g of SiO_2 support was used. A SiO_2 support with a surface area of 300 m^2/g, which was used for the ALE samples, was purchased from Aldrich. The SiO_2 support was preheated at 673 K for 16 h to stabilize the number of bonding sites and to remove physisorbed water. Cu(thd)$_2$ (thd = 2,2,6,6-tetramethyl-3,5-heptanedionate) was introduced at 413 K. The Cu(thd)$_2$ was then deposited on the SiO_2 support at 463 K over a reaction time of 8 h.

Two kinds of reduction pre-treatments for ALE-Cu/SiO_2 catalysts were used in this study. Low-temperature reduction was performed by calcination in air and by reduction in H_2 gas at 573 K for 5 h. The high-temperature reduction was carried out according to the following sequence of steps: (1) calcination at 573 K in air for 5 h; (2) reduction by temperature-programmed reduction (TPR) in 10% H_2/N_2 gas from 298 to 973 K; and (3) reduction at 773 K in H_2 gas for 5 h. The IM-Cu/SiO_2 samples used in this study were prepared by impregnating the SiO_2 from Aldrich Ltd. with an aqueous solution of Cu$(NO_3)_2$. The commercial Cu/ZnO/Al_2O_3 catalyst was manufactured by Süd-Chemie Catalysts, Inc. (catalyst #G66B), with a molar Cu/Zn/Al ratio of 30:60:10. The IM-Cu/SiO_2 and Cu/ZnO/Al_2O_3 catalysts were calcined in air and reduced in H_2 at 573 K for 5 h before use.

2.2. Catalytic activity measurements

All WGS reactions were carried out in a fixed-bed reactor (0.95 cm outer diameter) at atmospheric pressure. A thermocouple connected to a PID temperature controller was placed on top of the catalyst bed. Samples (50 mg) of catalyst were used for all WGS reactions, which were conducted by feeding a stream of CO/H_2O in a 1.1:1 feed molar ratio at 30 mL/min. The reactions were performed by pure CO stream with a total flow rate of 30 mL/min passing through liquid water at room temperature, and then the mixture of CO/H_2O passed over 50 mg catalyst. The flowing system of the reactor was heated with heating belts to avoid condensation of samples. All products were analyzed by gas chromatography (GC) on a 12-ft. Porapak-Q column using a thermal conductivity detector (TCD). The TOF was calculated by the formula [25]: TOF = [conversion × 0.25 (mL/s for CO) × 6.02×10^{23} (molecules/mol)]/[24400 (mL/mol) × 1.46×10^{19} (Cu sites/m^2)].

2.3. Temperature-programmed reduction (TPR)

H_2-TPR of catalysts was performed at atmospheric pressure in a conventional flow system. The ALE-Cu/SiO_2 catalyst was placed in a tube reactor and heated in a 10% H_2/N_2 mixed gas stream flowing at 30 mL/min at a heating rate of 10 K/min. The TCD current was 80 mA, and the detector temperature was 373 K. A cold trap containing a gel formed by adding liquid nitrogen to isopropanol in a Thermos flask was used to prevent water from entering the TCD.

2.4. Measurements of FT-IR spectra

In situ DRIFT analysis of CO adsorption and CO/H_2O co-adsorption on ALE-Cu/SiO_2 were performed with a Nicolet 5700 FTIR spectrometer fitted with a mercury–cadmium-telluride (MCT) detector operating at 1 cm^{-1} resolution and 256 scans. The DRIFT cell (Harrick Co.) was equipped with ZnSe windows and a heating cartridge that allowed samples to be heated to 773 K.

2.5. Temperature-programmed desorption (TPD)

TPD experiments were performed in a 100 mL/min stream of He at atmospheric pressure in a conventional flow system. The temperature was increased from 300 to 773 K at a rate of 10 K/min over the course of the TPD process. All signals were measured with a VG Smart IQ^+ 300D mass spectrometer. The temperature was measured with a K-type thermocouple inserted into the catalyst bed, and the desorbed products were admitted into the vacuum chamber through a leak valve using He as the carrier gas. The operating pressure in the chamber was approximately 3×10^{-7} Torr, and the base pressure in the chamber was approximately 2×10^{-9} Torr. H_2O and D_2O were dosed onto all catalysts by injection with a 10 μL Hamilton 7001 syringe through a port located at the upstream of the quartz reactor. The injection port, similar to that used in gas chromatography, was heated to 373 K to prevent the condensation of water.

2.6. Measurement of copper surface area

The specific Cu^0 surface area and dispersion of Cu catalysts were determined by N_2O chemisorption and TPR. All Cu^0 on catalysts was carefully oxidized in a 10% N_2O/N_2 stream according to the reaction: $2Cu_{(s)} + N_2O \rightarrow Cu_2O_{(s)} + N_2$.

The monolayer of Cu_2O on the catalyst surface after N_2O chemisorption was reduced using a TPR process. N_2O chemisorption was performed with a 10% N_2O/N_2 mixture flowing at 30 mL/min at 353 K. The TPR area of Cu_2O was quantified by sampling 1 mL of 10% H_2/N_2 to calculate the amount of N_2O consumed. The Cu^0 surface area could thus be calculated, assuming a N_2O/Cu molar stoichiometry of 0.5. The average surface density for Cu metal is 1.46×10^{19} copper atoms/m^2. The copper content of all catalysts was measured by inductively coupled plasma mass spectrometry (ICP/MS). As the amount of Cu atoms on the surface and the total Cu content of the catalyst were known, the copper dispersion could thus be calculated. The average particle size of Cu was calculated from Cu surface area by the formula: $d = 6V/A$.

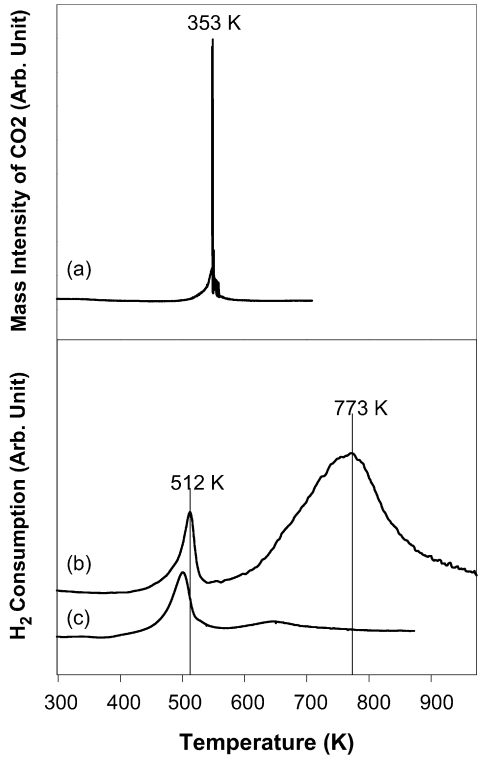

Fig. 1. (a) TPO profile of $Cu(thd)_2/SiO_2$ sample after $Cu(thd)_2$ was deposited on SiO_2; TPR profiles of catalyst after calcination in air at 573 K for 5 h: (b) 2.5% ALE-Cu/SiO_2 and (c) 2.5% IM-Cu/SiO_2.

2.7. Transmission electron microscopy (TEM)

High-resolution TEM analysis was carried out on a FEI Tecnai G2 F20 operating at 300 KeV and located at High Valued Instrument Center in the National Sun Yat-sen University, Taiwan. The catalyst samples after pretreatment were dispersed in methanol, and the solution was mixed ultrasonically at room temperature. A part of solution this solution was dropped on the grid for the measurement of TEM images.

3. Results

3.1. Temperature-programmed oxidation and reduction

Fig. 1 shows the TPO (temperature-programmed oxidation) and TPR (temperature-programmed reduction) profiles of the ALE-Cu/SiO_2 catalyst. Spectrum (a) is the mass spectrometric CO_2 signal obtained from the original $Cu(thd)_2/SiO_2$ sample oxidized to CuO/SiO_2, and shows a sharp CO_2 desorption peak at about 353 K. After TPO treatment, the sample was calcined in air at 573 K for 5 h. Fig. 1b shows the H_2-TPR profile of the oxidized 2.5% ALE-Cu/SiO_2 catalyst after calcination treatment. Two main peaks can be seen, with maxima at around 512 K and 773 K. It was found that the high-temperature peak corresponded to much greater H_2 consumption than the first reduction peak at 512 K. Similar results have also been presented in the literature, and have been interpreted in terms of complicated reduction steps [26–29]. The first peak at 512 K was consistent with the fact that the reduction of bulk CuO or Cu^{2+} to Cu^+ usually occurs at 528–573 K. The reduction peak at 773 K might be ascribed to the reduction of Cu^+ to Cu^0 or Cu species strongly bound to the SiO_2 support. Spectrum (c) depicts a TPR profile of 2.5% IM-Cu/SiO_2 catalyst after calcination. The first peak at the low temperature reveals similar reduction area to ALE-Cu/SiO_2 catalyst, but the high temperature peak at 773 K almost disappeared on IM-Cu/SiO_2. It is proposed to correspond to the typical reduction of bulk CuO to Cu^0.

Table 1
Comparison of the $Cu/ZnO/Al_2O_3$, IM-Cu/SiO_2, and ALE-Cu/SiO_2 catalysts.

Catalysts	Cu content (wt%)	Dispersion (%)	Particle size (nm)	Cu surface area (m^2/g)
$Cu/ZnO/Al_2O_3$	20	15	6.5	23
IM-Cu/SiO_2	10.3	8	17.6	7.3
IM-Cu/SiO_2	2.5	18	9.0	2.9
ALE-Cu/SiO_2	2.5	40	2.9	6.5

3.2. Activity tests

Table 1 lists the comparison in dispersion, Cu surface area, and Cu particle size for all Cu catalysts. About 40% dispersion was obtained with the 2.5% ALE-Cu/SiO_2 catalyst. The dramatic dispersion of the ALE-Cu catalyst was markedly larger than that of the 10.3% and 2.5% IM-Cu/SiO_2 catalysts preparation resulting from the typical impregnation method. The $Cu/ZnO/Al_2O_3$ catalyst gave the highest Cu surface area because of its higher copper content. The 10.3% IM-Cu/SiO_2 catalyst showed a slightly higher Cu surface area than ALE-Cu/SiO_2. The ALE-Cu/SiO_2 catalyst exhibited the smallest particle size compared to the other Cu catalysts. We performed TEM experiments on ALE-Cu/SiO_2, $Cu/ZnO/Al_2O_3$, 10% IM-Cu/SiO_2, and 2.5% IM-Cu/SiO_2 catalysts to observe the Cu particles, as shown in Fig. 2. The particle size of the ALE-Cu/SiO_2 catalyst was about 2.85 ± 0.32 nm, obtained by manually measuring the particles from TEM image (a) in Fig. 2. Large amounts of uniform and small nanoscale copper particles of ALE-Cu/SiO_2 were found in the TEM image (Fig. 2a).

The dependences of specific TOF and conversion versus temperature for the ALE-Cu/SiO_2, IM-Cu/SiO_2, and $Cu/ZnO/Al_2O_3$ catalysts are shown in Figs. 3A and 3B. The ALE-Cu/SiO_2 containing a low copper concentration revealed the effect of the Cu nanoparticles, showing dramatically high activity for the water gas shift reaction in comparison with the IM-Cu/SiO_2 and $Cu/ZnO/Al_2O_3$ catalysts, even at room temperature. The 10.3% IM-Cu/SiO_2 gave a copper surface area similar to that of 2.5% ALE-Cu/SiO_2, but exhibited very weak catalytic activity. The 10.3% and 2.5% IM-Cu/SiO_2 catalysts revealed no detectable activity below 423 K. The $Cu/ZnO/Al_2O_3$ catalyst gave the highest Cu surface area because of its higher copper content, and exhibited similar reaction conversion with ALE-Cu/SiO_2, as shown in Fig. 3B.

Arrhenius plots and apparent activation energies are shown for $Cu/ZnO/Al_2O_3$ and ALE-Cu/SiO_2 catalysts at 298 K–473 K (Fig. 3C).

3.3. FT-IR of CO adsorbed on ALE-Cu/SiO_2

We used CO as a probe molecule to identify the active sites on the ALE-Cu/SiO_2 catalyst, because it is a good probe molecule for vibrational spectroscopy and can usually provide important information about the surface sites of adsorbed species and the chemical environment of a copper surface. Fig. 4A shows the IR spectra of CO adsorbed on an ALE-Cu/SiO_2 catalyst following reduction treatment at 573 K for 5 h. The IR band of spectrum (a) may be assigned to linear CO adsorption on the Cu surface. The IR band could be fitted by two principal peaks, positioned at 2119 cm^{-1} (the L_1 state) and 2134 cm^{-1} (the L_2 state). The IR band of adsorbed CO rapidly diminished as the temperature was increased, and was scarcely discernible at 523 K. The IR band intensities of L_1- and L_2-CO decreased simultaneously with increasing temperature (Fig. 4B). Considering the H_2-TPR results, the pre-treatment reduction at 573 K might have led to partially reduced copper particles.

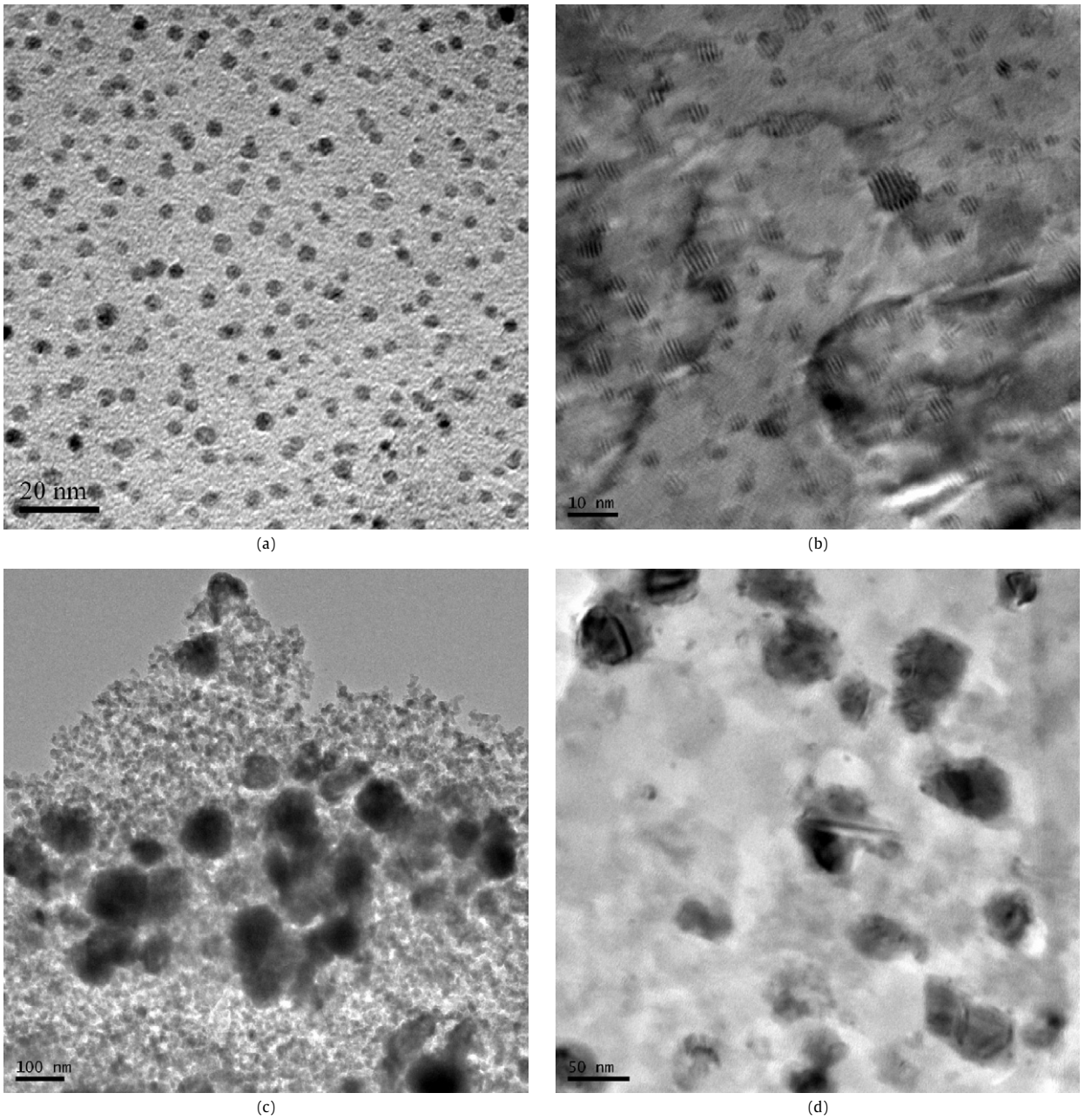

Fig. 2. TEM images of (a) ALE-Cu/SiO_2; (b) 20 wt% Cu/ZnO/Al_2O_3; (c) 10.3% IM-Cu/SiO_2; and (d) 2.5% IM-Cu/SiO_2.

Fig. 5 shows the IR spectra of CO adsorbed on the reduced ALE-Cu/SiO_2 catalyst, obtained by high-temperature reduction. This sample was assumed to be completely reduced. The difference between the spectra of CO adsorbed on the partially reduced copper surface and on the fully reduced ALE-Cu/SiO_2 would seem to suggest very different surface properties between the ALE-Cu/SiO_2 reduced at 573 K and that reduced at 773 K. The intensity of the IR of CO adsorption on completely reduced ALE-Cu/SiO_2 gradually decreased as the temperature was increased; however, a small amount of L_2-CO still remained on the Cu surface, even at 773 K, as shown in Fig. 5A. Fig. 5B shows the dependence of the integrated areas of both peaks (the L_1- and L_2-CO) in Fig. 5A versus temperature. One can see that L_1-CO had a larger relative intensity at 298 K, but it rapidly declined with increasing temperature. On the other hand, for the L_2-CO strongly bound on the copper surface, the intensity remained over the range 298–423 K, and then gradually decreased beyond 423 K.

3.4. In situ FTIR study of the rate of the WGS reaction on ALE-Cu/SiO_2

Fig. 6 displays the spectra obtained in time-dependence studies of the reaction of a saturation of adsorbed CO on differently pre-treated ALE-Cu/SiO_2 and IM-Cu/SiO_2 with H_2O at 298 K. CO adsorbed on the fully reduced ALE-Cu/SiO_2 (reduction at 773 K) almost disappeared within 3 min at room temperature when 5 μL of H_2O was injected into the reaction cell, as shown in Fig. 6B. However, there have been no reports in the literature that copper-based catalysts could provide high activity for the WGS reaction at room temperature, as observed for the ALE-Cu/SiO_2 catalyst used in this study. One can see that the IR bands of the L_1- and L_2-CO species were the major carbonyl components of the WGS reactions on each of the copper surfaces, and that these declined with time following the injection of 5 μL of H_2O. Fig. 6C reveals the identical experiment performed on 10.3% IM-Cu/SiO_2 for comparison with ALE-Cu/SiO_2, suggesting that large Cu particles offered much less efficiency for CO removal. The intensity of IR spectra of CO

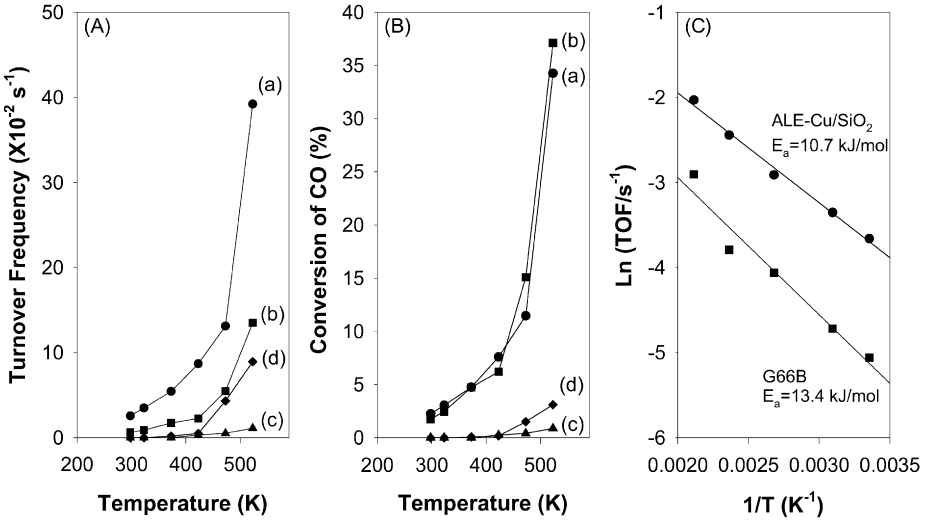

Fig. 3. Comparison of catalytic activity for the water–gas shift reaction for (A) turnover of frequency versus temperature and (B) CO conversion versus temperature: (a) 2.5% ALE-Cu/SiO_2; (b) 20% Cu/ZnO/Al_2O_3; (c) 10.3% IM-Cu/SiO_2; and (d) 2.5% IM-Cu/SiO_2 catalysts. (C) Arrhenius plots for Cu/ZnO/Al_2O_3 and ALE-Cu/SiO_2 at 298–473 K. The weight of catalyst used was 0.05 g.

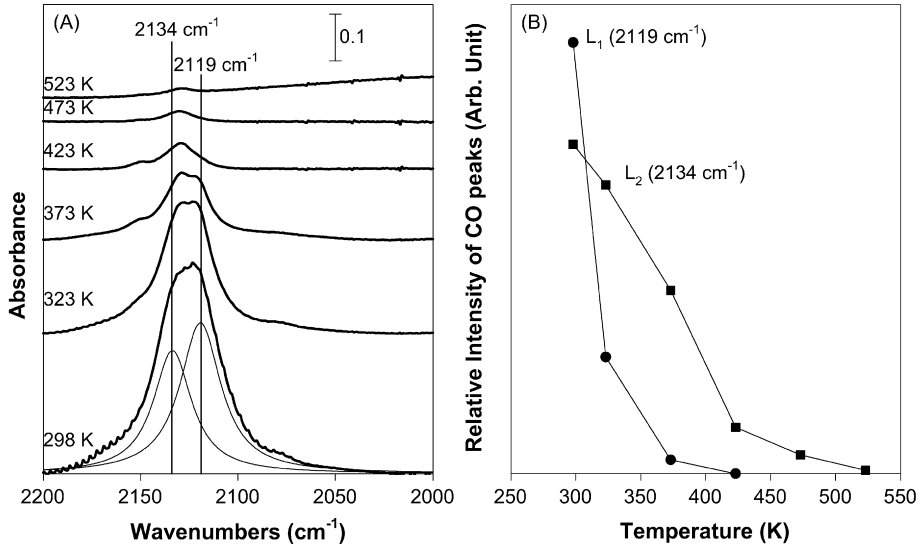

Fig. 4. (A) IR spectra of CO adsorbed on the low-temperature reduced ALE-Cu/SiO_2 catalyst at different temperatures. (B) Relative intensity of the L_1 and L_2 peaks of the CO band in part (A) with temperature.

adsorbed on the 10.3% IM-Cu/SiO_2 did not significantly decreased with time until 480 s. The difference of IR spectrum between curves 0 s and 480 s in Fig. 6C has shown in Fig. 6D, which contained weak intensity for L_1-CO and L_2-CO.

Fig. 7 shows the changes in the coverage of CO species on the copper surfaces in Fig. 6 as a function of time. The CO coverage was determined using the ratio of A/A_0, that A was the IR band area at different time and A_0 was the initial IR band area of saturated adsorption at 298 K. The CO coverage decreased linearly within 60 s for each of the copper catalysts, and the fully reduced ALE-Cu/SiO_2 (reduction at 773 K) apparently offered better initial rates for WGS reactions than either the partially reduced ALE-Cu/SiO_2 (reduction at 573 K) and IM-Cu/SiO_2. The spectra in Fig. 6, corresponding to the WGS reaction on the fully reduced ALE-Cu/SiO_2, were further analyzed with regard to the coverage of the L_1- and L_2-CO species versus time, as shown in Fig. 8. On the other hand, curves of the coverage of L_1- and L_2-CO from the pulse reactions on the fully reduced ALE-Cu/SiO_2 are shown in Fig. 9. The experiments were performed by injecting 0.1 μL of H_2O for each pulse after saturation adsorption of CO on the fully reduced ALE-Cu/SiO_2. As shown in Figs. 8 and 9, L_1-CO is obviously consumed faster than the L_2-CO species, implying that CO adsorbed at the L_1-sites reacted more rapidly with adsorbed water than the L_2-CO species.

Fig. 10 shows the low dosing amount of CO adsorbed on fully reduced ALE-Cu/SiO_2 with and without H_2O pre-adsorbed at 298 K. The low coverage of adsorbed CO was achieved by passing a pure 30 mL/min CO stream at atmospheric pressure for 1 min, and then passing a 30 mL/min helium stream for 30 min. Spectrum (a) shows the IR spectrum of CO on clean and reduced ALE-Cu/SiO_2, which indicates that the relative intensities for the two carbonyl species are L_2-CO > L_1-CO due to the low adsorption amount of CO. This means that the L_2 sites are filled before the L_1 sites. When the same dosing time of CO bound on the H_2O pre-covered Cu surface was used, the CO band showed an 18% reduction in intensity, while the L_2-CO band was less intense than that of L_1-CO, as shown in Fig. 10b. When the identical CO adsorption process was sequentially performed on the H_2O pre-covered Cu surface after

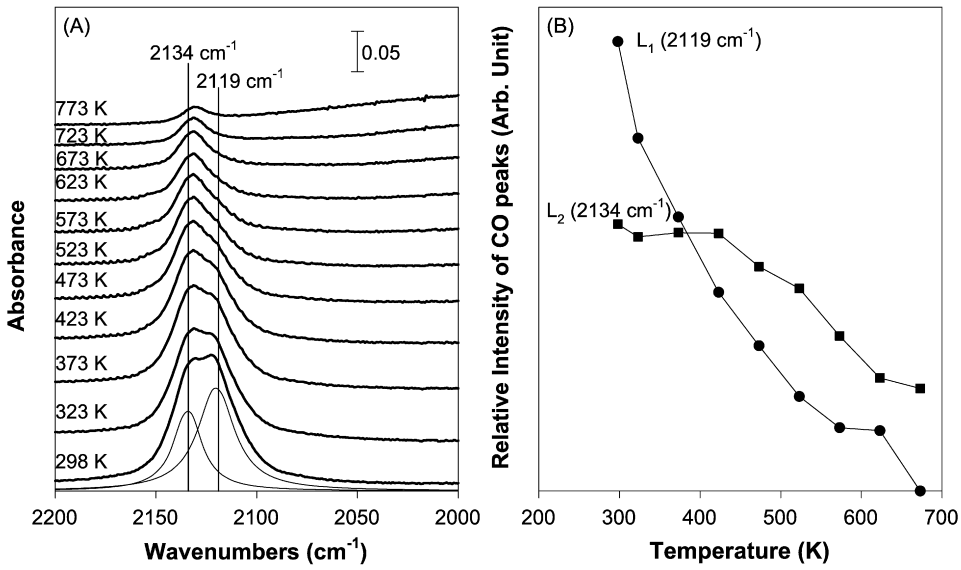

Fig. 5. (A) IR spectra of CO adsorbed on the high-temperature reduced ALE-Cu/SiO_2 catalyst at different temperatures. (B) Relative intensity of the L_1 and L_2 peaks of the CO band in part (A) with temperature.

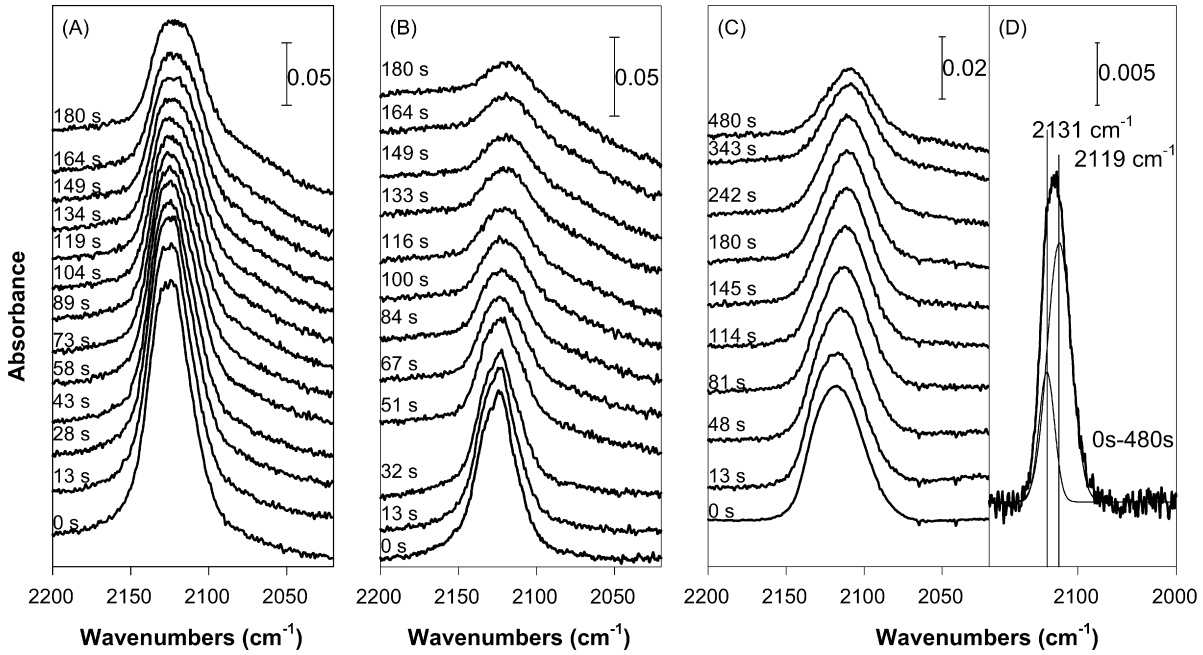

Fig. 6. Time-dependence of the IR spectra for co-adsorption of CO and H_2O on: (A) low-temperature reduction 2.5% ALE-Cu/SiO_2 catalyst, (B) high-temperature reduction 2.5% ALE-Cu/SiO_2 catalyst, and (C) 10.3% IM-Cu/SiO_2 catalyst. All samples were exposed to a 30 mL/min pure CO stream at atmospheric pressure for 30 min, followed by a 30 mL/min helium stream to purge the CO gas for 30 min, after which 5 μL of H_2O was injected into the reaction cell. (D) The difference of IR spectrum between curves at 0 s and 480 s in (C).

spectrum (b), one can see that the CO band gradually grew, which was accompanied by a concomitant decrease in the IR spectrum of adsorbed H_2O (Fig. 10, b–f).

Fig. 11 shows the dependence of the initial rate of the WGS reaction over the ALE-Cu/SiO_2 catalyst on the concentrations of CO and H_2O. All data were obtained from kinetic observations of the decreasing IR intensity of pre-adsorbed CO with time within 60 s as H_2O was added. As shown in Fig. 11a, when a constant amount of H_2O (5 μl) was injected onto the CO-covered ALE-Cu/SiO_2 catalyst, the initial rate could be enhanced by increasing the amount of CO adsorption. Interestingly, however, Fig. 11b shows that the initial rate was independent of the amount of H_2O injected for saturation CO coverage on ALE-Cu/SiO_2.

3.5. D_2O temperature-programmed desorption

We used the TPD to study the desorption behavior of D_2O and active sites on the ALE-Cu/SiO_2 catalyst. Fig. 12 displays the TPD spectra of D_2O from ALE-Cu/SiO_2 at various dosing concentrations, showing that the D_2O, HDO, and H_2O could be simultaneously monitored by quadrupole mass spectrometry in the course of the desorption process, which desorbed peaks at 373 and 586 K. At low dosing levels, initiated by dosing 1 μL of D_2O, the sample showed desorption at 373 K (curve (a)). The area of this peak reached a maximum after a 5 μL dosing amount. As the D_2O level increased, a peak at 586 K gradually developed, and two main peaks were observed, with maxima near 373 (α peak) and 586 K

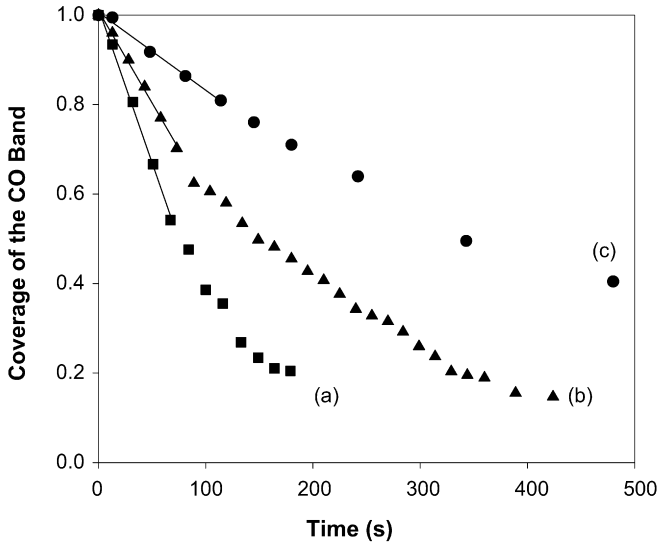

Fig. 7. Changes in the coverage of CO species as a function of time in Fig. 5: (a) high-temperature reduction ALE-Cu/SiO_2 catalyst; (b) low-temperature reduction ALE-Cu/SiO_2 catalyst; (c) 10.3% IM-Cu/SiO_2 catalyst.

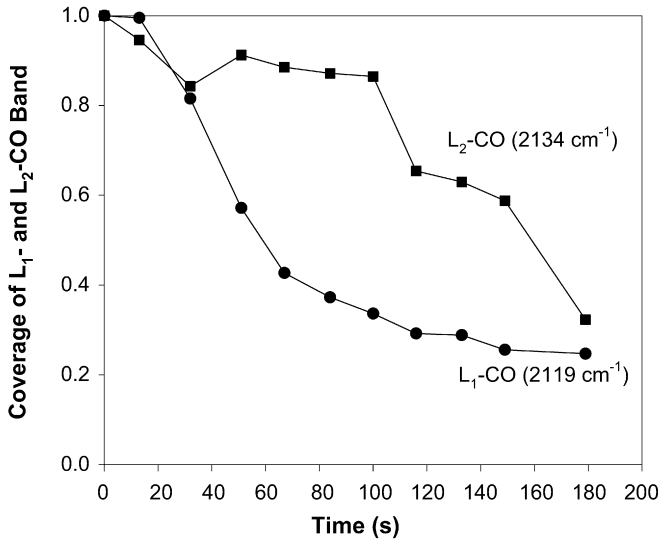

Fig. 8. Time-dependence of the relative intensities of the L_1- and L_2-CO peaks for co-adsorption of CO and H_2O on the high-temperature reduction ALE-Cu/SiO_2 catalyst in Fig. 5B.

(β peak). The identical TPD profiles of D_2O were also performed on the IM-Cu/SiO_2 catalyst prepared using a standard impregnation method, as shown in Fig. 13. Compared to Fig. 12, the weak signals of D_2O, HDO, and H_2O desorbed from the IM-Cu/SiO_2 catalyst, which is possibly ascribed to slight isotopic exchange between the deuterium atoms in water and SiOH. It is suggested that the IM-Cu/SiO_2 catalyst had difficulty binding D_2O on its surface.

Fig. 14 compares the desorption spectra of D_2O adsorbed on ALE-Cu/SiO_2 following various levels of CO dosing at 298 K. The ALE-Cu/SiO_2 sample with a 7 μL dosage of D_2O was fed by a CO stream at 100 mL/min, before the TPD experiments were done. It was found that the β states at 586 K could vanish faster than the α states at 373 K as the dosing amount of CO increased, implying that the water at the β state had higher reactivity with CO molecules than the water at the α state.

Fig. 15 shows the results of quadruple mass spectrometer monitoring of the WGS reactions on the ALE-Cu/SiO_2 catalyst at room temperature. The relationship between the adsorption states of

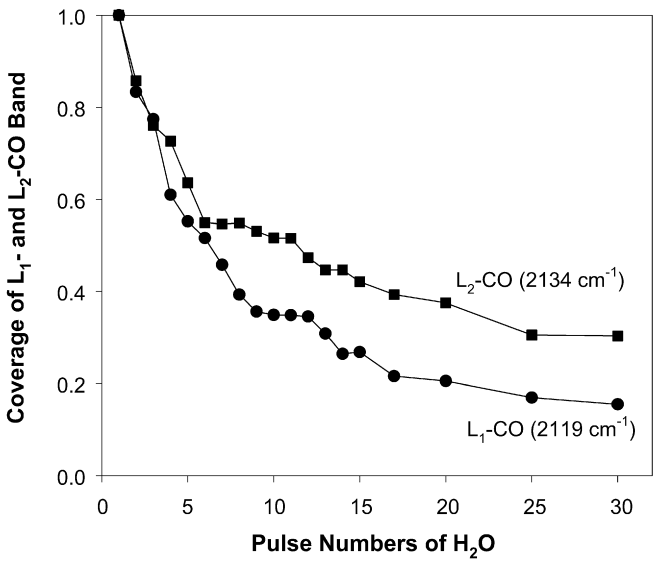

Fig. 9. Coverage of the L_1- and L_2-CO species as a function of the number of pulses of H_2O injected onto the high-temperature reduction ALE-Cu/SiO_2 catalyst with CO coverage. CO adsorption was achieved by exposure to a 30 mL/min pure CO stream for 30 min, followed a 30 mL/min helium stream for 30 min. 0.1 μL of H_2O was injected into the reaction cell for each co-adsorption.

H_2O and the WGS reaction was further investigated. After a dosing amount of 5 μL of H_2O, a 100 mL/min CO feed stream was passed through the H_2O-pre-covered ALE-Cu/SiO_2 catalyst at 298 K, leading to two evident mass signals of CO_2 being detected by QMS, as shown in spectrum (a). Both peaks of CO_2 formation in spectrum (a) could be considered to associate with adsorption sites on the ALE-Cu/SiO_2 surface. We elevated the temperature of the ALE-Cu/SiO_2 pre-covered by the injection of 5 μL H_2O to 473 K in helium in order to eliminate H_2O adsorbed on the α-sites (373 K), and cooled the catalyst to room temperature. This treatment led to β-H_2O (573 K) remaining on the ALE-Cu/SiO_2 surface, and the CO stream was passed through the ALE-Cu/SiO_2 catalyst. Spectrum (b) is the time profile of the mass spectrum of CO_2, showing that the sharp peak that formed rapidly could still be observed and retained at a similar mass intensity to spectrum (a), but the broad and weak CO_2 signal generated later completely disappeared. No detectable H_2 signals were observed during the WGS reactions.

4. Discussion

4.1. Chemical state on reduced ALE-Cu/SiO_2

The TPR profile of the oxidized ALE-Cu/SiO_2 catalyst featured two reduction peaks at 512 K and 773 K. In several previous papers [25–29], it has been speculated that the reactions involved in the reduction process might be the following:

$$CuO + H_2 \rightarrow Cu^0 + H_2O, \quad (1)$$

$$Cu^{2+} + (1/2)H_2 \rightarrow Cu^+ + H^+, \quad (2)$$

$$Cu^+ + (1/2)H_2 \rightarrow Cu^0 + H^+. \quad (3)$$

Reactions (1) and (2) occur at lower temperatures than reaction (3). In general, the reduction temperature of small particles of CuO is lower than that of bulk CuO [30]. The reduction of large CuO particles usually occurs at about 540 K, and highly dispersed CuO is reduced more easily than larger CuO particles [30]. In addition, some literature reports have indicated that the reduction temperature of a well-dispersed (3–5 nm) CuO/SiO_2 catalyst prepared by an ion-exchange method can be below 523 K [31]. The ion-exchange method may result in the formation of Cu–O–Si

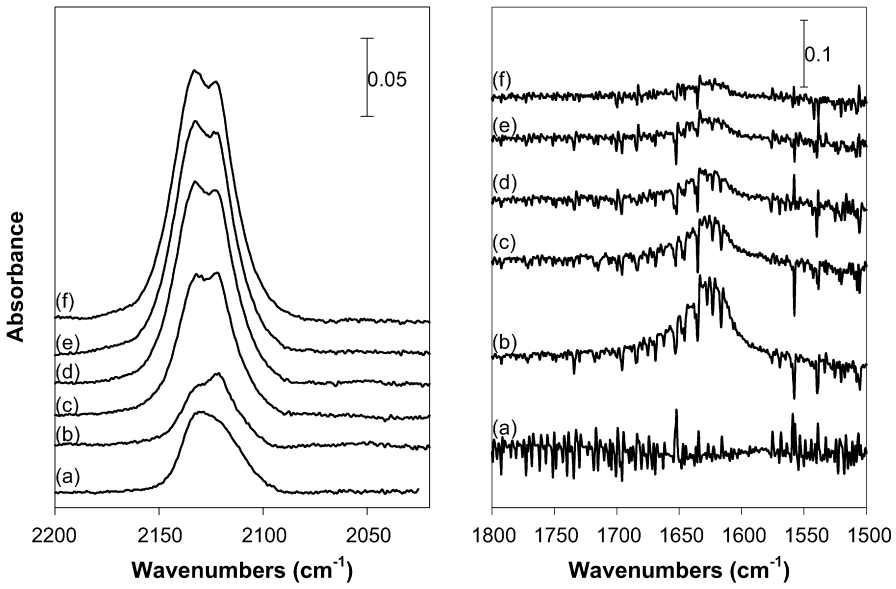

Fig. 10. CO adsorbed on fully reduced ALE-Cu/SiO_2 with and without 5 μL of H_2O dosing at 298 K. The CO adsorption was carried out in a pure 30 mL/min CO stream at atmospheric pressure for 1 min, and then a 30 mL/min helium stream was passed for 30 min. (a) CO adsorption on clean ALE-Cu/SiO_2 without H_2O; (b) CO adsorption on H_2O pre-covered ALE-Cu/SiO_2; (c) CO adsorption after (b); (d) CO adsorption after (c); (e) CO adsorption after (d); (f) CO adsorption after (e).

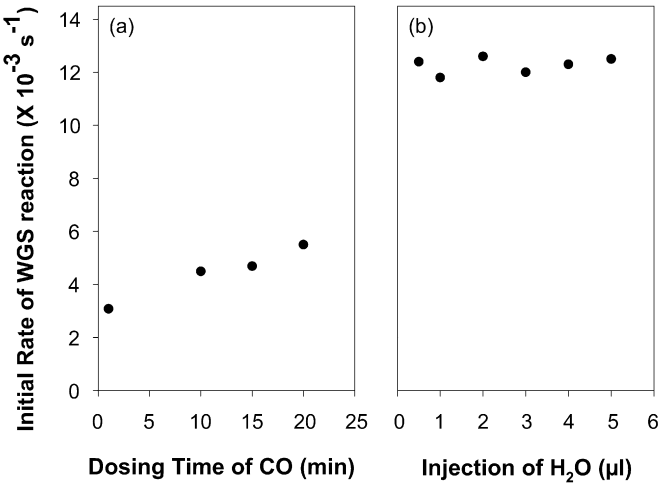

Fig. 11. Dependence of the initial rate of the WGS reaction on the ALE-Cu/SiO_2 catalyst: (a) different dosing time of CO at a constant injection volume of H_2O, and (b) different injection volumes of H_2O at a constant CO coverage.

species during the preparation of the Cu/SiO_2 catalyst. The reduction of Cu^{2+} to Cu^+ for the Cu–O–Si species has been identified to occur at 523 K, which strongly overlapped with the peak for the reduction of small particles of CuO to Cu^0 [30]. The further reduction of Cu^+ to Cu^0 for Cu–O–Si species required a temperature above 873 K [31].

In the present TPR profile, shown in Fig. 1, the low-temperature peak at 512 K could reasonably be assigned to the one-step reduction of Cu^{2+} to Cu^0 of highly dispersed CuO particles or the partial reduction of isolated Cu^{2+} to Cu^+ ions in a two-step reduction process. The second peak at the higher temperature was attributed to a second reduction path from Cu^+ to Cu^0, which was due to a highly dispersed form of copper interacting strongly with the silica surface, but a similar reduction peak at 773 K was not observed on 2.5% IM-Cu/SiO_2. The copper nanoparticles apparently behave very differently from their bulk forms, possibly because of electronic and structural effects of the materials. However, on the surface of the copper, it might be difficult to avoid oxygen perturbation from the hydroxyl groups of silica, even if the catalyst has been reduced at 773 K for 5 h. Some authors have indicated that the small Cu particles or isolated Cu atoms on oxide supports could be rendered partially electropositive as a result of interaction with oxygen atoms at the surface of the support, even if the copper is reduced [32,33]. Some authors have also reported that the electronic structure of copper is size-dependent. Copper has a completely filled 3d band ($4s^13d^{10}$) and no d-states at the Fermi level. The valence band may shift toward a higher binding energy as a result of reduced Cu particle size [12]. Chen et al. indicated that small particles of Cu led to an increase in work function [13]. The smaller Cu particles produced by the ALE method might have a partially filled 3d band with a high density of states at the Fermi level, thereby resulting in lower electron density.

4.2. Band assignments of IR spectra

The high activity for the WGS reaction shown by the fully reduced ALE-Cu/SiO_2 catalyst is strongly indicated to be associated with active sites on the copper surface. Assignments of the IR bands of CO adsorbed on a reduced Cu surface have been proposed [32,34]. IR bands below 2100 cm^{-1} were assigned to CO adsorbed on low index planes, such as the (111) and (100) faces [32–34], while the band at 2102–2118 cm^{-1} was assigned to CO adsorbed at imperfect sites, such as step and edge sites. Bands above 2120 cm^{-1} might be from CO adsorbed on highly dispersed supported copper particles [34–36]. On the other hand, stretching frequencies of CO adsorbed on copper have also been found to occur in different regions for each oxidation state. In general, peaks located at above 2140 cm^{-1} can be attributed to Cu^{2+} sites [37]. The band of CO adsorbed on Cu^+ sites has been reported to appear at 2110–2135 cm^{-1} [37].

The above review of the assignments of the stretching frequencies of CO adsorbed on copper sites does not seem to distinguish the L_1- and L_2-CO in terms of the electronic and structural effects of copper. We repeatedly performed TPR experiments on ALE-Cu/SiO_2 samples following high-temperature reduction pretreatment (773 K). No reduction peak was observed in the H_2-TPR experiments for any of the reduced ALE-Cu/SiO_2 catalysts, implying that the sample was likely to have been completely reduced. On the basis of the above description, the IR spectra of CO adsorbed

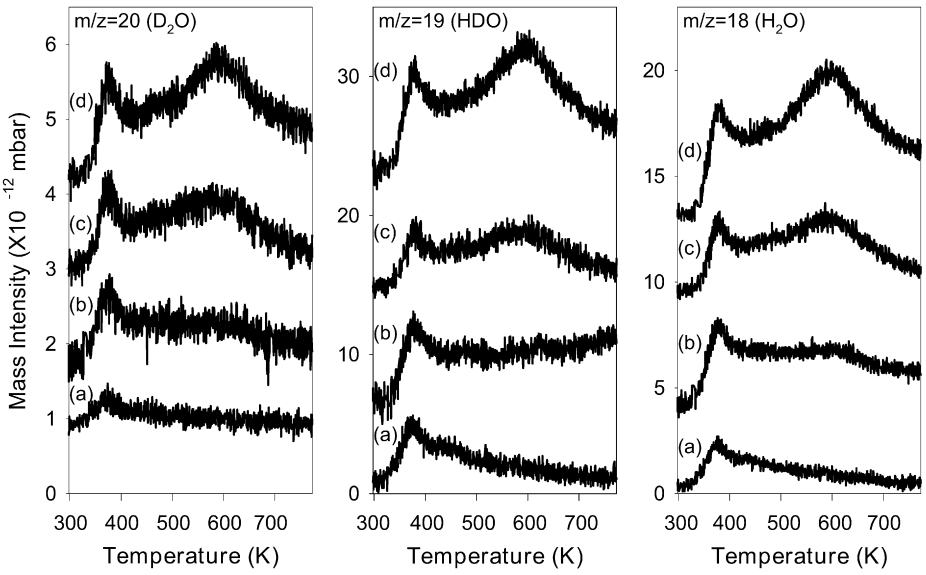

Fig. 12. TPD spectra of D_2O, HDO, and H_2O from the ALE-Cu/SiO_2 catalyst with various dosing amounts of D_2O: (a) 1 μL; (b) 3 μL; (c) 5 μL; (d) 7 μL.

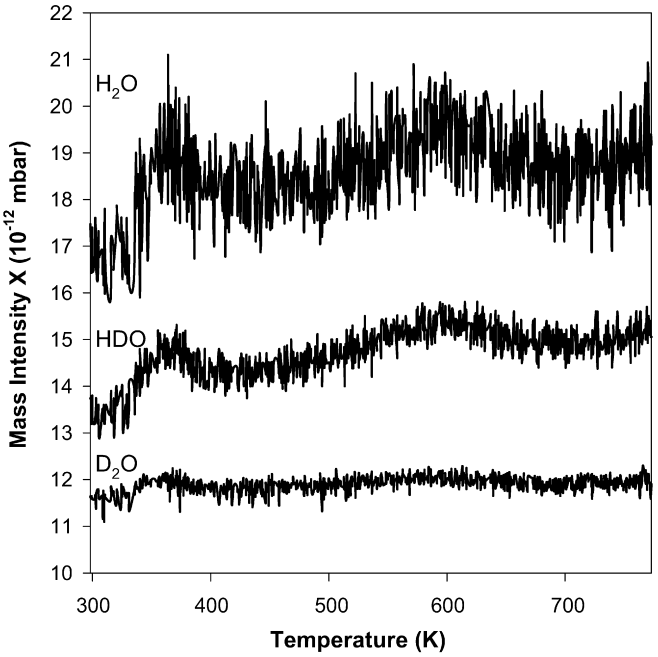

Fig. 13. TPD spectra of D_2O, HDO, and H_2O from the IM-Cu/SiO_2 catalyst with a 7 μL D_2O dosage.

on the ALE-Cu/SiO_2 catalyst tended towards a higher stretching frequency of 2134 cm^{-1} (L_2-CO), which might stem from the effect of nanoscale copper particles. The L_1 sites for CO adsorption could be reasonably assigned to the imperfect sites on the surface.

4.3. Relationship between CO adsorption and the WGS reaction

From the results of CO adsorbed on ALE-Cu/SiO_2 at different temperatures, the L_2 sites showed a stronger binding ability for CO than the L_1 sites. FT-IR studies of co-adsorption experiments of CO and H_2O (Figs. 8 and 9) have shown that two types of atop sites for CO adsorption on the ALE-Cu/SiO_2 surface dominated the rate during the WGS reaction. The respective carbonyl species (L_1- and L_2-CO) displayed a large difference in the rates at which they underwent the WGS reaction. The rate of coverage loss for L_1-CO was evidently faster than that for L_2-CO when H_2O was added to CO pre-covered ALE-Cu/SiO_2 at 298 K. This implied that L_1-CO at defect sites (sites giving rise to CO stretching at 2119 cm^{-1}) was highly active in the WGS reaction. The CO adsorbed at L_2 sites, i.e., the small particle and/or isolated copper atom sites, was still available for the WGS reaction, but obviously proved to be less efficient.

4.4. Relationship between water adsorption and the WGS reaction

The TPD spectra of D_2O, H_2O, and HDO showed the same two types of desorption states at 373 and 586 K on the ALE-Cu/SiO_2, as shown in Fig. 12. The D_2O strongly dissociated on copper nanoparticles resulted in rapid isotopic exchange between D_2O and SiOH. The H–D isotopic exchange of D_2O obviously occurred before the H_2O and HDO species desorbed from the ALE-Cu/SiO_2 surface. A D_2O molecule was first dissociated on the copper surface to atomic deuterium and then migrated onto the support surface. It can be deduced that there is a strong interaction between spillover deuterium and SiOH. Fig. 14 clearly shows that β-H_2O reacts more easily with CO than with α-H_2O. On the other hand, Fig. 15 also reveals that the first and second CO_2 peaks could closely depend on β- and α-H_2O species, respectively. The β-H_2O can be attributed to the mainly dominant species in the WGS reaction.

The IR spectra of the co-adsorption of CO and H_2O in Fig. 10 can further provide some information to discriminate these active sites for adsorbed H_2O. Spectrum (a) obviously gave a higher intensity of L_1-CO than that of L_2-CO. When a CO stream was passed through the H_2O-precovered ALE-Cu/SiO_2 for 60 s, the β-H_2O species could perform the WGS reaction with CO, and α-H_2O remained on the ALE-Cu/SiO_2 surface. This leads to the conclusion that the L_1-CO had a larger IR intensity, as seen in spectrum (b) in Fig. 10. As the CO dosage increased, α-H_2O was consumed by adsorbed CO, while L_2-CO significantly grew, as shown in spectra (c)–(f). Thus, it can reasonably be proposed that the active sites of the adsorbed α- and β-H_2O species might be associated with the L_2 and L_1 sites, respectively.

4.5. Factors of ALE-Cu/SiO_2 enhanced WGS reaction

The mechanism of the WGS reaction over Cu-based catalysts has been extensively discussed, but it remains controversial. Two models, namely the redox and associative mechanisms, have been

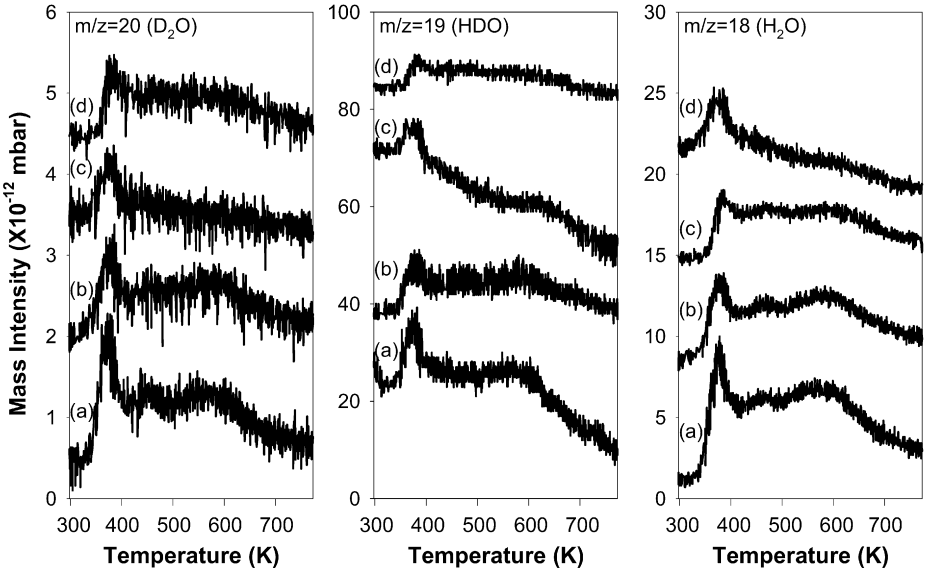

Fig. 14. TPD spectra of D_2O, HDO, and H_2O from the ALE-Cu/SiO_2 catalyst after D_2O was adsorbed on the ALE-Cu/SiO_2 following various levels of CO dosing at 298 K (a) 30 s; (b) 60 s; (c) 300 s; (d) 600 s. The ALE-Cu/SiO_2 sample with a 7 μl dosage of D_2O was fed by a CO stream at 100 mL/min before the TPD experiments were performed.

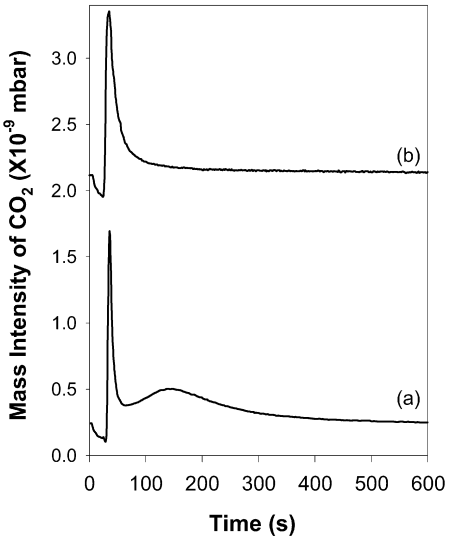

Fig. 15. Mass spectra of CO_2 obtained by a 100 mL/min CO stream passing over different H_2O pre-covered ALE-Cu/SiO_2 catalysts at 298 K: (a) injecting 5 μL of H_2O onto the reduced ALE-Cu/SiO_2 catalyst at 298 K in a 100 mL/min helium stream; (b) elevating the temperature of the ALE-Cu/SiO_2 catalyst to 473 K in helium after a 5 μL H_2O dosage, and then cooling the catalyst to room temperature.

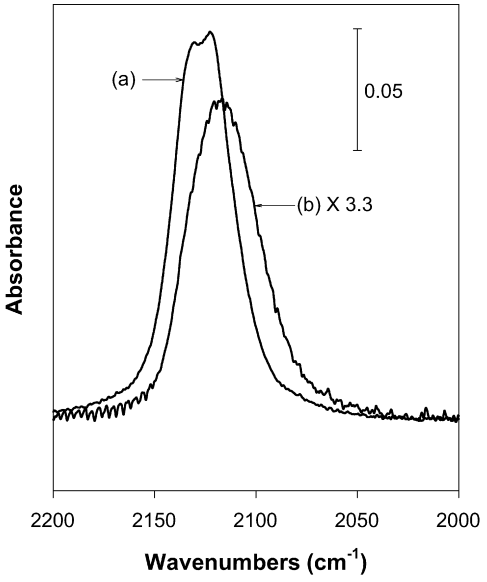

Fig. 16. IR spectra of CO adsorbed on (a) 2.5% ALE-Cu/SiO_2 and (b) 10.3% IM-Cu/SiO_2 catalyst at room temperatures. All samples were exposed to a 30 mL/min pure CO stream at atmospheric pressure for 30 min, followed by a 30 mL/min helium stream to purge the CO gas for 30 min.

proposed to explain the mechanism of the WGS reaction on a copper surface [38–47]. The redox mechanism for the WGS reaction involves the oxidation of CO on the surface by atomic oxygen derived from H_2O dissociation [39–41]. In the associative mechanism, it is suggested that the surface hydroxyls (OH groups) formed from H_2O on a copper surface combine with adsorbed CO to produce reaction intermediates such as formate, carbonate, or carboxyl, which then decompose to H_2 and CO_2 [42–45].

Fig. 15 shows that no detectable H_2 signal was observed in the course of the WGS reaction. We compared the relative responses of CO_2 and H_2 in the mass spectrometer by sampling 1 mL of CO_2/H_2 in a 1:1 volume ratio, and found that the ratio of the mass signals of CO_2 and H_2 was about 6.2. Thus, the loss of the H_2 signal in Fig. 15 was obviously independent of the instrumental response of the mass spectrometer for different molecules, and could only be interpreted in terms of a low likelihood of the WGS reaction proceeding through the formate pathway. On the other hand, it is noteworthy that no observable reaction intermediates such as formate, carbonate, or carboxyl species were adsorbed during the co-adsorption of CO and H_2O for the WGS reaction on the ALE-Cu/SiO_2 surface, as shown in Fig. 10. Rather, these data provided evidence for the feasibility of a redox-type reaction mechanism on the ALE-Cu/SiO_2.

Fig. 16 compares the saturation of adsorbed CO on ALE-Cu/SiO_2 and IM-Cu/SiO_2 catalysts at 298 K, showing that IM-Cu/SiO_2 provided lower intensity for CO adsorption than ALE-Cu/SiO_2 did. On the other hand, the IR spectrum of CO adsorbed on IM-Cu/SiO_2 obviously shifted to lower vibrational frequency, implying that larger Cu particles mainly contained sites on low index planes, such as the (111) and (100) faces. Nevertheless, Fig. 6D shows that L_1- and L_2-CO remained the major species for the WGS reaction. Undoubtedly, an ALE-Cu/SiO_2 catalyst can provide many more L_1- and

L_2-sites to bind CO due to its high dispersion and small particles, leading to high efficiency for WGS reaction. The 10.3 wt% IM-Cu/SiO_2 catalyst has a similar copper surface area as the 2.5 wt% ALE-Cu/SiO_2 catalyst but apparently provided poor ability for water dissociation and CO adsorption [24]. However, water dissociation will always be the essential part of the WGS reaction. Some authors have studied the WGS reaction on copper surfaces using density functional calculations, showing that copper nanoparticles can provide more active sites for the WGS reaction than Cu(100) [44]. It is suggested that copper nanoparticles contain far more low-coordinated corner and edge sites than a flat copper surface, and can have better CO binding and water dissociation [44]. Our experimental results have elucidated that the defect sites for L_1-CO on the ALE-Cu/SiO_2 catalyst are of fundamental importance to the catalytic activity of the supported copper nanoparticles for the adsorbed CO and H_2O. This can explain why the ALE-Cu/SiO_2 catalyst can provide stronger activity for water dissociation and water gas shift reactions than IM-Cu/SiO_2, even though both catalysts have similar Cu surface areas.

Some studies have cited the dissociation of H_2O as the rate-determining step on Cu [8,42], but the ALE-Cu/SiO_2 catalyst undoubtedly behaved in a different way to traditional Cu-based catalysts, in that it readily decomposed H_2O. This was the key factor in the ALE-Cu/SiO_2 catalyst showing high activity for the WGS reaction at room temperature. Interestingly, Fig. 11 shows that the reaction rate of a saturation coverage of adsorbed CO was independent of the H_2O concentration, suggesting that a strong dissociation reaction of H_2O might occur on the ALE-Cu/SiO_2 surface. The nature of copper nanoparticles also might influence water dissociation. Wang et al. studied water dissociation on a clean oxygen pre-adsorbed copper surface by means of theoretical calculations [47], and showed that the barrier to reaction on the oxygen-covered copper surface was lower than that on a clean copper surface. It has been reported that the formation of the H_2O–OH complex is the driving force for lowering the barrier to water dissociation on copper surfaces [48]. For water dissociation on oxygen pre-adsorbed metal surfaces, adsorbed oxygen abstracts hydrogen from water to produce hydroxyls ($H_2O + O \rightarrow 2OH$) [47]. Our results have shown that copper nanoparticles produced by the ALE method interact strongly with the SiO_2 support, leading to a partial positive charge on the copper surface. This phenomenon is deduced to be the essential factor for inducing and enhancing water dissociation, leading to the observed high reactivity for the WGS reaction.

5. Conclusions

We have prepared uniform copper nanoparticles (2.85 ± 0.32 nm) on a silica support through application of the atomic-layer-epitaxy technique (ALE). The IR spectra of CO adsorbed on the ALE-Cu/SiO_2 catalyst (Cu/SiO_2 catalyst prepared by the atomic-layer-epitaxy technique) revealed two major active sites on the copper surface, namely defect sites (sites for L_1-CO with an IR spectrum at 2119 cm^{-1}) and highly dispersed Cu particles and/or isolated Cu atoms sites (sites for L_2-CO with an IR spectrum at 2134 cm^{-1}). The relative adsorption strength of CO at the L_2-sites is higher than that at the L_1-sites, but the water gas shift reaction mainly occurs at the L_1-sites, corresponding to defect sites on small particles. It is also proposed that H_2O adsorbed on defect sites can enhance the water gas shift reaction. The high efficiency of the water gas shift reaction on the ALE-Cu/SiO_2 catalyst may be ascribed to its strong activity in promoting H_2O dissociation. We speculate that the small Cu particles or isolated Cu atoms may have strong interactions with the SiO_2 support, leading to a partially electropositive state as a result of interactions with oxygen atoms at the surface of the support, even if the copper is reduced. The low electron density of the copper surface may strongly induce water dissociation and facilitate the conversion of CO to CO_2 and H_2.

Acknowledgments

Financial support from the National Science Council of the Republic of China (NSC 96-2113-M-182-002-MY2) is gratefully acknowledged. We would like to thank Liang-Chu Wang for the operation in the HRTEM. Dr. Pin C. Yao is acknowledged for operating the F-120C ALE equipment in the material and chemical research laboratories at the Industrial Technology Research Institute.

References

[1] H. Iida, A. Igarashi, Appl. Catal. A 298 (2006) 52.
[2] T. Tabakova, F. Boccuzzi, M. Manzoli, J.W. Sobczak, V. Idakiev, D. Andreeva, Appl. Catal. A 298 (2006) 127.
[3] M. Rønning, F. Huber, H. Meland, H. Venvik, D. Chen, A. Holmen, Catal. Today 100 (2005) 249.
[4] F.C. Meunier, A. Goguet, C. Hardacre, R. Burch, D. Thompsett, J. Catal. 252 (2007) 18.
[5] D. Tibiletti, A. Amieiro-Fonseca, R. Burch, Y. Chen, J.M. Fisher, A. Goguet, C. Hardacre, P. Hu, D. Thompsett, J. Phys. Chem. B 109 (2005) 22553.
[6] C.H. Kim, L.T. Thompson, J. Catal. 230 (2005) 66.
[7] G. Jacobs, E. Chenu, P.M. Patterson, L. Williams, D. Sparks, G. Thomas, B.H. Davis, Appl. Catal. A 258 (2004) 203.
[8] X. Wang, J.A. Rodriguez, J.C. Hanson, D. Gamarra, A. Martínez-Arias, M. Fernández-García, J. Phys. Chem. B 110 (2006) 428.
[9] V. Matolín, L. Sedláček, I. Matolínová, F. Šutara, T. Skála, B. Šmíd, J. Libra, V. Nehasil, K.C. Prince, J. Phys. Chem. B 112 (2008) 3751.
[10] B. White, M. Yin, A. Hall, D. Le, S. Stolbov, T. Rahman, N. Turro, S. O'Brien, Nano Lett. 6 (2006) 2095.
[11] J.S. Garitaonandia, M. Insausti, E. Goikolea, M. Suzuki, J.D. Cashion, N. Kawamura, H. Ohsawa, I.G.D. Muro, K. Suzuki, F. Plazaola, T. Rojo, Nano Lett. 8 (2008) 661.
[12] Z. Pászti, G. Petö, Z.E. Horváth, A. Karacs, L. Guczi, J. Phys. Chem. B 101 (1997) 2109.
[13] P. Chen, X. Wu, J. Lin, K.L. Tan, J. Phys. Chem. B 103 (1999) 22.
[14] L. Porte, M. Phaner-Goutorbe, J.M. Guigner, J.C. Bertolini, Surf. Sci. 424 (1999) 262.
[15] Y.H. Kim, D.K. Lee, H.G. Cha, C.W. Kim, Y.C. Kang, Y.S. Kang, J. Phys. Chem. B 110 (2006) 24923.
[16] M. Yin, C.K. Wu, Y. Lou, C. Burda, J.T. Koberstein, Y. Zhu, S. O'Brien, J. Am. Chem. Soc. 127 (2005) 9506.
[17] B.S. Lim, A. Rahtu, G. Gordon, Nat. Mater. 2 (2003) 749.
[18] A. Kytökivi, J.P. Jacobs, A. Hakuli, J. Meriläinen, H.H. Brongersma, J. Catal. 162 (1996) 190.
[19] L.B. Backman, A. Rautiainen, A.O.I. Krause, M. Lindblad, Catal. Today 43 (1998) 11.
[20] P. Mäki-Arvela, L.P. Tiainen, M. Lindblad, K. Demirkan, N. Kumar, R. Sjöholm, T. Ollonqvist, J. Väyrynen, T. Salmi, D.Y. Murzin, Appl. Catal. A 241 (2003) 271.
[21] M. Lashdaf, A.O.I. Krause, M. Lindblad, M. Tiitta, T. Venäläinen, Appl. Catal. A 241 (2003) 65.
[22] A. Hakuli, A. Kytökivi, A.O.I. Krause, Appl. Catal. A 190 (2000) 219.
[23] C.S. Chen, J.H. Lin, J.H. You, C.R. Chen, J. Am. Chem. Soc. 128 (2006) 15950.
[24] C.S. Chen, J.H. Lin, T.W. Lai, Chem. Commun. (2008) 4983.
[25] J. Nakamura, I. Nakamura, T. Uchijima, Y. Kanai, T. Watanabe, M. Saito, T. Fujitani, J. Catal. 160 (1996) 65.
[26] E.D. Guerreiro, O.F. Gorriz, J.B. Rivarola, L.A. Arrúa, Appl. Catal. A 165 (1997) 259.
[27] E.D. Guerreiro, O.F. Gorriz, G. Larsen, L.A. Arrúa, Appl. Catal. A 204 (2000) 33.
[28] G.V. Shanbhag, T. Joseph, S.B. Halligudi, J. Catal. 250 (2007) 274.
[29] C. Torre-Abreu, M.F. Ribeiro, C. Henriques, G. Delahay, Appl. Catal. B 12 (1997) 249.
[30] L.F. Chen, P.J. Guo, M.H. Qiao, S.R. Yan, H.X. Li, W. Shen, H.L. Xu, K.N. Fan, J. Catal. 257 (2008) 172.
[31] A.J. Marchi, J.L.G. Fierro, J. Santamaría, A. Mozón, Appl. Catal. A 142 (1996) 375.
[32] P. Hollins, Surf. Sci. Rep. 16 (1992) 51.
[33] F. Boccuzzi, A. Chiorino, G. Martra, M. Gargano, N. Ravasio, B. Carrozzini, J. Catal. 165 (1997) 129.
[34] F. Coloma, F. Marquez, C.H. Rochester, J.A. Anderson, Phys. Chem. Chem. Phys. 2 (2000) 5320.
[35] F. Boccuzzi, S. Coluccia, G. Martra, N. Ravasio, J. Catal. 184 (1999) 316.
[36] F. Boccuzzi, G. Martra, C. Partipilo Papalia, N. Ravasio, J. Catal. 184 (1999) 334.
[37] A. Dandekar, M.A. Vannice, J. Catal. 178 (1998) 621.
[38] A.A. Gokhale, J.A. Dumesic, M. Mavrikakis, J. Am. Chem. Soc. 130 (2008) 1402.
[39] D.S. Newsome, Catal. Rev. Sci. Eng. 21 (1980) 275.

[40] E. Fiolitakis, H. Hofmann, J. Catal. 80 (1983) 328.
[41] N.A. Koryabkina, A.A. Phatak, W.F. Ruttinger, R.J. Farrauto, F.H. Ribeiro, J. Catal. 217 (2003) 233.
[42] J. Nakamura, J.M. Campbell, C.T. Campbell, J. Chem. Soc. Faraday Trans. 86 (1990) 2725.
[43] C.T. Campbell, K.A. Daube, J. Catal. 104 (1987) 109.
[44] P. Lih, J. Rodriquez, J. Chem. Phys. 126 (2007) 164705.
[45] C.V. Ovesen, B.S. Clausen, B.S. Hammershøi, G. Steffensen, T. Askgaard, I. Chorkendorff, J.K. Nørskov, P.B. Rasmussen, P. Stoltze, P. Taylor, J. Catal. 158 (1996) 170.
[46] T. Shido, Y. Iwasawa, J. Catal. 141 (1993) 71.
[47] G.C. Wang, S.X. Tao, X.H. Bu, J. Catal. 244 (2006) 10.
[48] K. Andersson, G. Ketteler, H. Bluhm, S. Yamamoto, H. Ogasawara, L.G.M. Pettersson, M. Salmeron, A. Nilsson, J. Am. Chem. Soc. 130 (2008) 2793.